PHYSICAL REVIEW B **80**, 115336 (2009)

Origin and limiting mechanism of induced nonequilibrium currents in gated two-dimensional electron systems

N. Ruhe, G. Stracke,* Ch. Heyn, and D. Heitmann
Institut für Angewandte Physik und Mikrostrukturforschungszentrum, Universität Hamburg, Jungiusstrasse 11, D-20355 Hamburg, Germany

H. Hardtdegen and Th. Schäpers
Institute of Bio- and Nanosystems (IBN-1), JARA Jülich-Aachen Research Alliance, and Virtual Institute of Spinelectronics (VISel), Research Centre Jülich GmbH, D-52425 Jülich, Germany

B. Rupprecht, M. A. Wilde,† and D. Grundler
Lehrstuhl für Physik funktionaler Schichtsysteme, Physik Department, Technische Universität München, James-Franck-Str. 1, D-84747 Garching bei München, Germany

(Received 22 June 2009; revised manuscript received 25 August 2009; published 30 September 2009)

We have studied experimentally the nonequilibrium currents (NECs) induced by sweeping either the magnetic field B or the carrier density n_S of a two-dimensional electron system (2DES). The gated 2DES resided in a modulation-doped GaAs/$Al_xGa_{1-x}As$ heterostructure and was integrated into a micromechanical cantilever. The NECs provoke a magnetic moment which we have detected via torque magnetometry down to 300 mK. Additional electrical leads allowed for simultaneous magnetotransport measurements. We find a hysteretic behavior of the NECs and a striking asymmetry of the corresponding magnetic moment around integer filling factors $\nu = hn_S/eB$. Surprisingly, the shape of the hysteresis loops is the same for sweeps of B or n_S if plotted versus ν. In a certain parameter regime each NEC signal exhibits a characteristic slope which is found to depend only on the filling factor at large B or n_S. Based on a model considering capacitive coupling between 2DES and gate we attribute the slopes to the conductance quantization of the quantum Hall effect. The NECs are found to be limited by the time-dependent buildup of the radial Hall field governed by the gate capacitance. These findings are in contrast to a floating 2DES without a gate where the breakdown of the quantum Hall effect was previously reported to limit the NECs. Our model also explains the observed shape and dependence on temperature as well as sweep rate. The *in situ* measurement of the longitudinal resistance allows us to directly correlate the magnetic behavior with both the magnetic field and temperature-dependent resistance of the 2DES.

DOI: 10.1103/PhysRevB.80.115336 PACS number(s): 71.10.Ca, 71.70.Di, 73.20.At, 73.23.Ra

I. INTRODUCTION

The orbital magnetization M of a two-dimensional electron system (2DES) consists of two contributions M_{eq} and M_{NEC} at mK temperatures, i.e., quantum oscillations of the de Haas–van Alphen (dHvA) effect and magnetic signals induced by nonequilibrium eddy currents (NECs), respectively. The dHvA effect is an equilibrium effect which has already been studied under various conditions. In high magnetic fields B pronounced dHvA oscillations have been reported for integral[1–4] and fractional quantum Hall (QH) states[5] in single-layered 2DESs. Such oscillations provide at low temperature T fundamental information about, both, the density of states and ground state energy U of the 2DES.[6–8] At $T=0$, the thermodynamic equilibrium magnetization M_{eq} is given by $M_{eq}=-(\partial U/\partial B)_{n_S}$ (n_S is the carrier density) and includes all manybody effects.[9–11] The magnetization M_{NEC} due to NECs induced by a sweeping magnetic field is a nonequilibrium effect that changes sign as a function of sweep direction of B. The mechanism limiting the induced currents in a *floating* 2DES is attributed to the breakdown of the QH effect.[12] NECs have been explored in detail recently[13–18] and valuable information about the QH effect breakdown has been gained. For a recent review see Ref. 19. In studies on 2DES with moderate mobility the hysteretic NEC signal was found to be symmetric around the position of an integer filling factor $\nu = n_S/(eB/h)$.[20] Very recently, the experimental observation of M_{NEC} induced by sweeping the *carrier density* n_S of a 2DES has been reported by Faulhaber *et al.*[21] These authors observed an asymmetry of the NECs around integer ν. A decade before, Dolgopolov *et al.*[22] reported magnetogalvanic measurements on Corbino-type 2DESs. These authors found a field-dependent voltage between inner and outer contacts that was hysteretic with B, increased linearly with B in a certain field regime and was asymmetric with respect to integer ν.[22] The absolute signal strength depended on the capacitance of the electrical leads and the electrometer. Hysteretic phenomena due to NECs were also present in investigations using single-electron transistors addressing the local chemical potential of QH states.[23,24] A direct correlation between these earlier observations and NECs in magnetization experiments has not been reported so far. A comparison has only recently become possible due to the development of sensitive torque magnetometers with integrated leads and gates for a 2DES.[21,25]

In this paper, we investigate systematically the generation of NECs as a function of B and n_S on the same 2DES for both, sweeping magnetic field and sweeping carrier density.

The simultaneous measurement of the magnetotransport properties allows us to directly correlate M_{NEC} with the magnetoresistance of the gated 2DES. The observed characteristics are in strong contrast to the behavior of NECs in floating 2DESs.[19] In particular, (i) the NECs are smaller by one order of magnitude if compared to a floating 2DES prepared from the same wafer and (ii) the magnetic moment has a strongly asymmetric shape as a function of ν. We find (iii) a similar behavior of NEC signals induced by $\partial n_S/\partial t$ and $\partial B/\partial t$ if plotted against ν. (iv) At large B the NEC signal shows a universal behavior and depends linearly on $\partial n_S/\partial t$ and $\partial B/\partial t$ in a certain parameter regime. Findings (i) and (ii) imply that a mechanism different from the QH effect breakdown dominates the NECs in a gated 2DES.

Combining the magnetization and magnetotransport data we develop a detailed understanding of the mechanism leading to NECs in the presence of a field-effect electrode. The model based on capacitive charging[13,22] which we adapt and develop further explains the observed hysteresis in major and minor loops as well as the temperature dependence. We argue here, that NECs in gated 2DESs arise due to a field-induced charge buildup. The signal strength is limited by the gate capacitance and *not* by the QH effect breakdown. We point out that the model is consistent with the orthodox picture of how NECs are generated in floating 2DESs,[19] where the capacitive coupling between redistributed electrical charges is much smaller and not limiting the NECs.

The paper is organized as follows. In Sec. II we describe the experimental details. In Sec. III we present experimental magnetization data obtained on gated 2DES and compare them with the floating case. In Sec. IV we develop a detailed model that can explain the observed behavior. We apply the model to the dependence of the NECs on temperature and sweep rate in Sec. V and conclude with Sec. VI.

II. EXPERIMENT: FIBER-OPTICS MAGNETOMETRY AND MAGNETOTRANSPORT ON THE SAME 2DES

In this paper we report on magnetization experiments performed using a micromechanical cantilever magnetometer incorporating a 2DES with electrical contacts and a field-effect gate electrode (sample A, cf. Fig. 1). Utilizing an optical readout based on a glass fiber interferometer[25,26] we monitored the magnetization M with a high sensitivity of 5×10^{-16} J/T at $B=10$ T and at $T=300$ mK. The 2DES was formed in a modulation-doped GaAs/$Al_xGa_{1-x}As$ heterojunction and integrated into a 3.5-μm-thick GaAs micromechanical cantilever. The spacer width between the doping layer and the 2DES was 20 nm. The fabrication of cantilever magnetometers was reported elsewhere.[27] The rectangular 2DES of area $A_{2\mathrm{DES}}=1.15$ mm^2 was provided with a 20 nm Au field-effect electrode and four thermally alloyed AuGe/Ni contacts at the corners. The magnetometer included a calibration coil for absolute determination of the magnetization data. All leads were connected via Al bonds to the wiring in the ^{3}He cryostat. We applied a voltage V_{gate} to tune n_S via the field effect.

The magnetization M was measured in a homogeneous field B supplied by an axial superconducting magnet. The

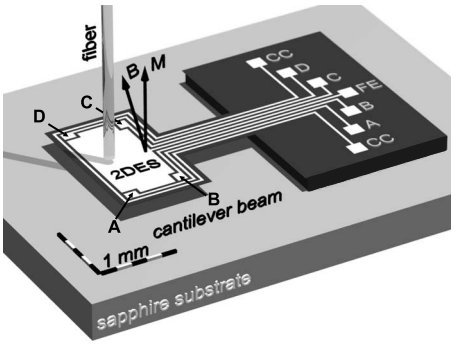

FIG. 1. Sketch of the micromechanical cantilever magnetometer (sample A) with the fiber-optics interferometer used for readout of the cantilever deflection. The rectangular 2DES mesa is integrated at the end of the cantilever beam. The magnetization M_{NEC} of the NECs is perpendicular to the 2DES plane. The cantilever normal is tilted by an angle of 15° with respect to B. Contacts CC: calibration coil, A–D: 2DES transport contacts, FE: field-effect electrode.

normal of the 2DES plane was tilted by an angle α of 15° with respect to B, resulting in a torque $\tau=M\times B$ acting on the cantilever beam. An optical fiber was glued to a piezoceramic tube and adjusted at a constant distance to the cantilever surface by a voltage V_{piezo}. We used our fiber-optics interferometer as a null detector to measure the deflection of the cantilever. Details of this experimental setup were described in Ref. 26. The magnetization is given by $M=K(V_{\mathrm{piezo}}-V_{\mathrm{piezo},B=0})/(B\sin 15°)$. K is the calibration constant which is determined by feeding a current through the calibration coil. Due to the alloyed contacts, the setup from Fig. 1 allowed us to perform magnetization [cf. Fig. 2(a)] and magnetotransport measurements [cf. Fig. 2(b)] simultaneously. We used V_{gate} to vary the electron density n_S in the experiments between 5×10^{14} and 33×10^{14}/m^2. When presenting the V_{gate}-dependent data we will give the corresponding value of $n_s=[V_{\mathrm{gate}}(V)+0.41\ \mathrm{V}]7.55\times10^{15}/(\mathrm{m}^2\ \mathrm{V})$ and not V_{gate} for clarity. For the magnetotransport measurements an AC current $I=50$ nA with frequency $f=37$ Hz was applied between contacts B and C in Fig. 1 and the voltage was measured between contacts A and D. Here, the gate and the 2DES were kept at the same potential. For comparison we will exemplarily show magnetization data obtained on 2DESs without field-effect electrodes and without contacts. As a reference we show data from 2DESs realized in two different further heterostructures. Sample B has a structure similar to sample A, i.e., it is based on a modulation-doped GaAs/$Al_xGa_{1-x}As$ heterojunction. Sample C is a 2DES formed in a InGaAs/InP heterostructure.[28] This set of reference data is chosen to illustrate that floating 2DESs exhibit in general NECs that are qualitatively different from the NECs in gated samples. All measurements were performed at 300 mK unless explicitly stated otherwise.

III. EXPERIMENTAL DATA ON NONEQUILIBRIUM CURRENTS IN GATED AND FLOATING 2DES

Magnetization data of a gated 2DES (sample A) and a floating 2DES from a different wafer (sample B) are dis-

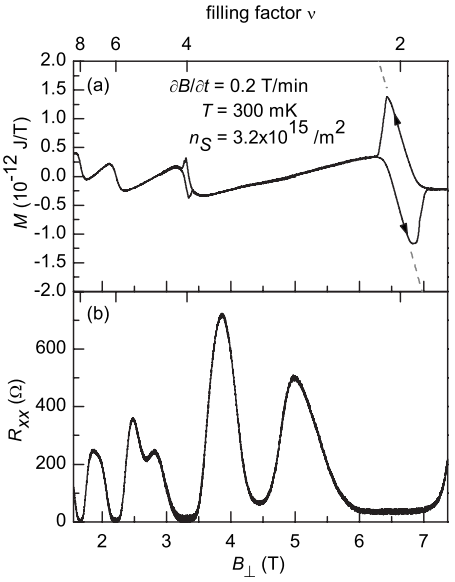

FIG. 2. (a) DHvA oscillations and NECs measured in a gated 2DES with transport contacts (sample A) at $T=300$ mK. Arrows indicate the sweep direction of B. $B_\perp$ is the component of the magnetic field B normal to the 2DES. The NECs in the gated 2DES are pronouncedly asymmetric around integer filling factors ν. The maxima of the NECs are shifted behind the position of integer ν with respect to the sweep direction. The NEC signal varies linearly around integer ν, i.e., the slope $\partial M/\partial B$ is constant as indicated by the dashed lines. (b) Longitudinal resistance oscillations measured simultaneously to the magnetization M. The longitudinal resistance shows pronounced minima at integer ν. The small offset from zero resistivity (R_{parasit}) is due to a parasitic parallel conductance arising from the continuous laser illumination of the fiber-optics interferometer. This will be considered in the evaluation.

played in Figs. 2(a) and 3, respectively. In both samples M_{NEC} as well as the equilibrium dHvA effect are well resolved. M_{NEC} can be clearly distinguished from the dHvA signal because it flips sign depending on the sweep direction, whereas the dHvA effect is a thermodynamic equilibrium

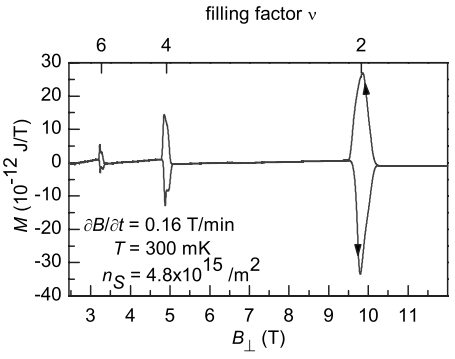

FIG. 3. DHvA oscillations and NECs in a floating 2DES, i.e., a 2DES without gate electrode and without contacts (sample B) at $T=300$ mK. Arrows indicate the sweep direction of B. Note that the NEC signal is much more symmetric around $\nu=2$ than in case of the gated 2DES [Fig. 2(a)]. These data are representative for the generic behavior of NECs observed on a large number of floating 2DESs by different authors.

phenomenon and thereby is independent of the sweep direction. In the following we focus on the NEC signal M_{NEC}.

The signal strength and variation as a function of B are markedly different for the floating and the gated 2DES. The NECs of the floating 2DES are a factor of ~20 larger than in the sample with contacts and gate. Disregarding small disturbances the NECs in Fig. 3 are roughly symmetric around integer ν. In contrast the NECs of the gated 2DES in Fig. 2(a) are found to be asymmetric: the maxima of the NECs do not appear at integer filling factors ν but are shifted behind the position of integer ν with respect to the sweep direction, i.e., the maximum of the NEC is shifted to higher (smaller) magnetic fields B in the up sweep (down sweep). The NECs vary linearly, i.e., with a constant slope $\partial M/\partial B$ around integer ν [dashed gray lines in Fig. 2(a)]. In Sec. IV we will attribute the observed asymmetry to the gate and electrical contacts attached to the 2DES. Up and down sweeps exhibit the same slope [dashed gray lines] over a broad regime. Only for the lowest sweep rates an additional substructure becomes visible, leading to different slopes for up and down sweeps.

Interestingly, we generate NECs also at a *constant* magnetic field when we vary the carrier density n_S through V_{gate}. Such a behavior was reported in Ref. 21. In Fig. 4 we compare NECs around $\nu=2$ generated by (a) a sweeping field B for different fixed values of n_S and (b) a variation in V_{gate} for different fixed values of B. The data show striking similarities. In both cases we observe the same asymmetry and a constant slope $dM/d\nu$ (indicated by dashed lines) of the NEC signal. The values of $dM/d\nu$ are identical for a given ν above a critical density and a critical field. Only for small n_S and B the behavior deviates from the characteristic slope.

Before we develop a model that explains this behavior we would like to present additional experiments. To study the hysteretic behavior of M_{NEC} in further detail we have performed minor-loop measurements. Data for the gated sample A are shown in Fig. 5. The extremal hysteresis curve for a full field sweep is shown in black. Several minor loops, where the sweep direction has been reversed inside the hysteresis, are shown as gray lines. Strikingly, the extremal loop and all minor loops have nearly the same slope at $\nu=2$ and reach their maximum at the same magnetic-field position (indicated by the dotted vertical line). For comparison we show minor loop measurements on a floating 2DES (sample C) in Fig. 6. The behavior is strikingly different: upon reversal of the sweep direction the NEC signal in the floating sample B abruptly changes sign and approaches the other extremal curve.

As we discuss below, these two different observations suggest a different current-limiting mechanism for the gated sample. In Fig. 7(a) we display M around $\nu=2$ for different temperatures T. We find that M_{NEC} decreases rapidly with T. At about 4 K the signal has reduced to zero. (Here, the dHvA oscillation is still pronounced. This again underscores their different origin.) The NEC amplitude ΔIA that was defined in Fig. 4(a) is plotted in Fig. 7(b). We observe a nonlinear T dependence with shoulders in the limits of low temperature as well as high temperature. This behavior will be correlated with the simultaneously measured magnetotransport data. It is important to note that contacts to the 2DES and an applied

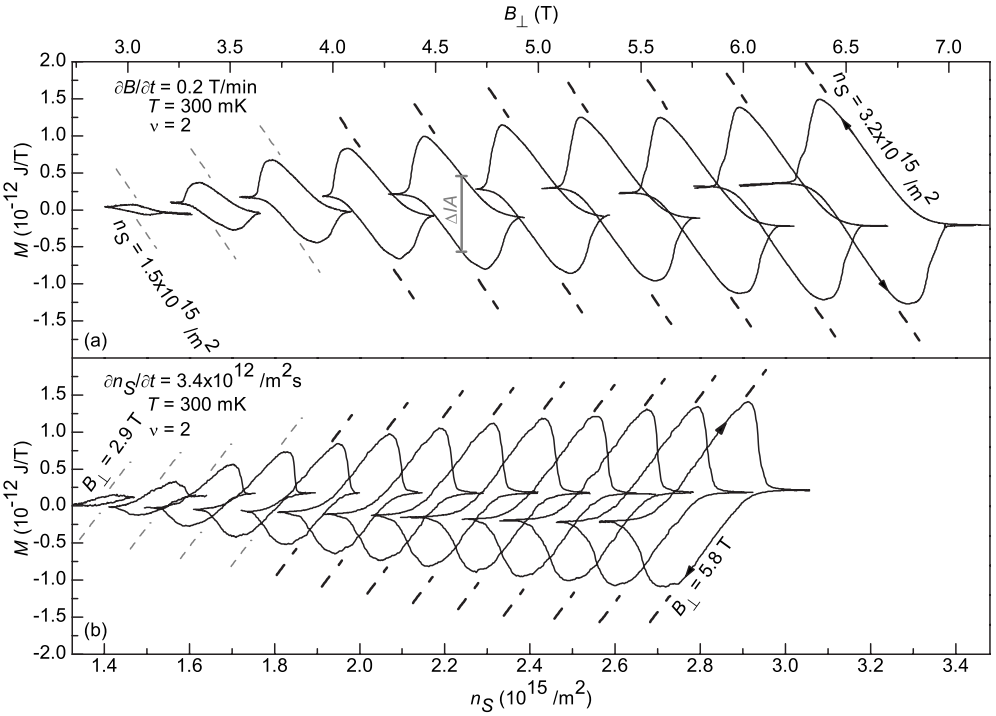

FIG. 4. (a) Magnetization M highlighting the NECs induced by $\partial B/\partial t = \pm 0.2$ T/min for different carrier densities n_S at $T = 300$ mK. The carrier density n_S is kept constant for each measurement and is incremented by $\Delta n_S \approx 1.9 \times 10^{14}/\mathrm{m}^2$ between the measurements. The definition of the NEC amplitude ΔIA, i.e., the maximum difference of the NEC signal between up and down sweeps is shown exemplarily in gray. (b) M for different fixed magnetic fields B at $T = 300$ mK. Here, n_S was varied with a rate of $\partial n_S/\partial t = \pm 3.4 \times 10^{12}/\mathrm{m}^2$ s. The magnetic field B is changed by $\Delta B \approx 0.24$ T in a step-wise manner between the measurements. In (a) and (b) we focus on the hysteretic behavior of M_{NEC} in the regime of $\nu = 2$. Arrows indicate the sweep direction of B or n_S, respectively. At high magnetic fields $B_\perp > 3.8$ T the slope of M as indicated by the dashed lines has a constant value. Below $B_\perp < 3.8$ T the data fall below the indicated slope. No NECs are observed at small magnetic fields $B_\perp < 2.7$ T.

bias current do not suppress the NECs. Vice versa, no sign of the NEC signal is seen in the magnetotransport data. This means that although NECs can be *generated* by adding or removing charge via the contacts, the nonequilibrium currents themselves are decoupled from the contacts, i.e., they

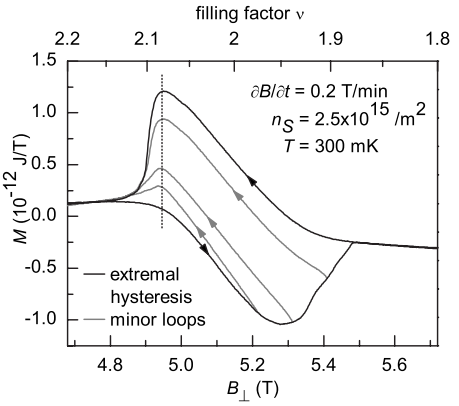

FIG. 5. Minor loop measurements of M around $\nu = 2$ in the *gated* sample A. Arrows indicate the sweep direction. The extremal hysteresis is shown in black, the minor loops in gray. The minor loops have nearly the same slope at $\nu = 2$. As discussed in Sec. IV this indicates the back transfer of the redistributed charges at a constant rate. The minor loops reach their maxima at the same magnetic field B (dotted line).

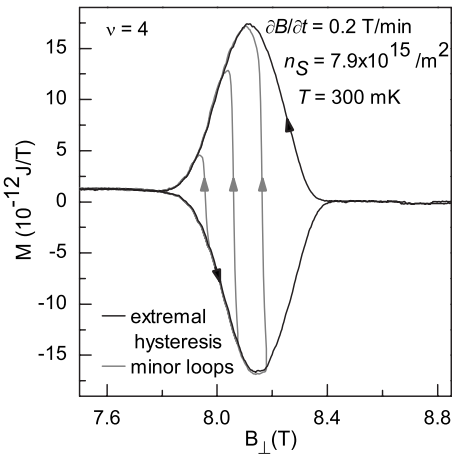

FIG. 6. Minor loop measurements of M in a floating 2DES around $\nu = 4$ (sample C). Arrows indicate the sweep direction. The extremal hysteresis is shown in black, the minor loops in gray. The minor loops display a nearly vertical slope and saturate only when approaching the extremal curve. This behavior can be explained by current limiting mechanisms that are discussed in the framework of the QHE breakdown (cf. Ref. 19). Note that this floating 2DES also shows an NEC amplitude that is (i) one order of magnitude larger if compared to the gated 2DES in Fig. 2(a) and (ii) of the same order of magnitude if compared to the floating 2DES in Fig. 3. This underscores that the high NEC amplitude is a generic property of NECs observed on floating 2DESs.

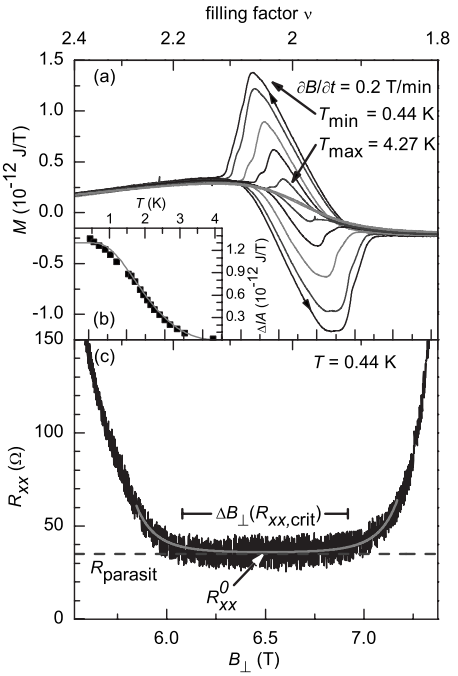

FIG. 7. (a) Magnetization M of magnetic-field-dependent NECs for different temperatures T. For clarity only every fourth curve is shown. Arrows indicate the sweep direction. (b) Temperature dependence of the NEC amplitude ΔIA. The NECs reduce for higher temperatures T due to the relaxation of E_r as a result of the increasing conductivity σ_{xx}. The fit to the data will be discussed in Sec. V A. (c) Longitudinal resistivity minimum (black) measured simultaneously in van der Pauw geometry. A reciprocal Gaussian curve (gray) has been fitted to the data to extract the minimum R^0_{xx} and the width $\Delta B_\perp$ of the region where $R_{xx}<R_{xx,\mathrm{crit}}$. The background R_{parasit} is caused by parasitic parallel conductivity due to the continuous laser illumination from the laser interferometer.

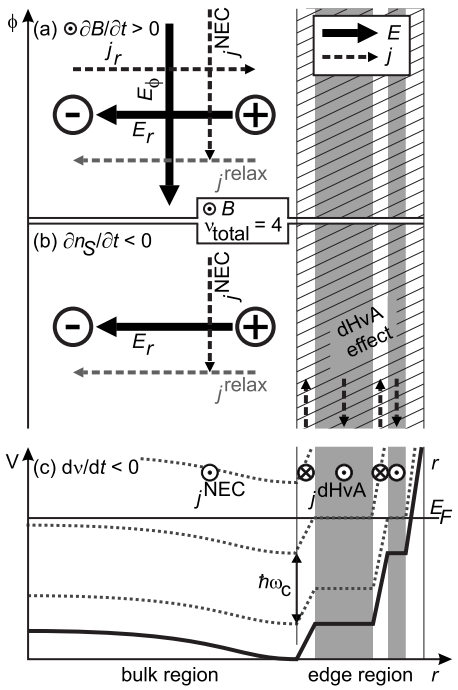

FIG. 8. Sketch of our model for the generation of NECs. The total filling factor is $\nu=4$. The bulk is incompressible whereas on the sample edge compressible and incompressible strips (Ref. 29) are formed. In the compressible and incompressible strips alternating equilibrium currents flow, causing the equilibrium magnetization of the dHvA effect (Ref. 34). (a) Sweeping the perpendicular magnetic field induces an azimuthal electric field E_ϕ. In the QHE regime, this leads to a radial current density $j_r=\sigma_{xy}E_\phi$, i.e., a charge transfer (Ref. 22) between the center and the edge of the sample. The charge transfer builds up a radial electric field E_r which drives the NEC j^{NEC}. In real samples, where $\sigma_{xx}=0$ does not strictly hold, a current j^{relax} will reduce the electric field E_r and lead to a decay of the NEC over time once the field sweep is stopped. (b) Changing the carrier density n_S yields a radial electric field E_r in the incompressible bulk of the sample. The NEC is induced due to this field E_r analogous to (a). Reversal of the sweep direction yields reversed electric fields and therefore NECs j^{NEC} with different signs in (a) and (b). (c) Sketch of electrostatic energy V. On the right hand side we assume compressible and incompressible strips following Refs. 29 and 30. On the left the bending of the electrostatic energy V in the incompressible bulk of the sample is depicted assuming a radial electric field profile. This sketch follows Refs. 17 and 22.

do not interact with the bias-induced transport currents essential to monitor the QHE. Before we discuss the magnetotransport data [cf. Fig. 2(b)] in detail, it is instructive to present the microscopic model for M_{NEC} which we have developed.

IV. NECs IN A GATED 2DES—MODEL CONSIDERATIONS

For our model we divide the 2DES into an outer region (edge region) and a central region (bulk region). Let us first assume that these parts coexist independently. The equilibrium currents j^{dHvA} in the compressible and incompressible strips[29] are responsible for the equilibrium magnetization of the dHvA effect.[30] According to the results of spatially resolved experiments in Refs. 31 and 32 the currents flow near the edge around integer ν. They are confined to the incompressible strips.[33] Klaffs *et al.*[24] deduced that the NECs flow in the innermost incompressible strip. Indeed, assuming a superimposed NEC in the sample edge should cause a self-consistent shift of the compressible and incompressible strips and the current in the strips would remain the same. We assume for the model developed below that the NECs are located in the innermost incompressible strip.

For the sketch in Fig. 8 it is convenient to consider a circular sample. We can then subdivide the currents **j** and electric fields **E** into their orthogonal components along the radial and azimuthal direction. The sweeping magnetic field $\partial B/\partial t=-\nabla\times E_\phi$ induces an azimuthal electric field E_ϕ [Fig. 8(a)]. Since the Hall angle is 90° in an ideal QHE state, the azimuthal field leads to a *radial* current which is $j_r=-\nu e^2/h\cdot E_\phi$ at integer ν. This current transfers charge in the incompressible bulk of the sample and builds up the radial electric field E_r, which increases linearly with the increment of B in the regime where σ_{xx} is vanishingly small.[22] The NEC $j^{\mathrm{NEC}}=\sigma_{xy}\cdot E_r$ is driven by this radial electric field E_r.[17] A sketch of the resulting electrostatic energy V is shown in Fig. 8(c) (we define V as the electrostatic energy in order to

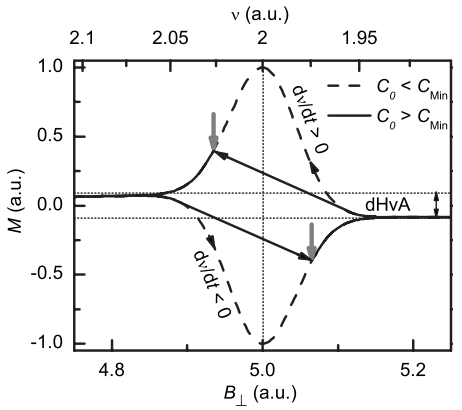

FIG. 9. Sketch: magnetization M of a NEC for two different values of C_0. We assume $\sigma_{xx}=0$ and hence no relaxation. The relation between the jump in the dHvA effect and the NEC is not to scale. $C_0 < C_{\mathrm{Min}}$ (dashed line): the 2DES is floating, the NEC signal reaches the extremal curve which is limited by the QHE breakdown. $C_0 > C_{\mathrm{Min}}$ (solid line): the 2DES is gated and the NEC is limited by the charge transfer rate (constant slope) until the extremal curve is reached.

reserve E for electrical fields). The slope of the linear increase in E_r depends on the value of ν because of the quantized conductivity on the one hand and on the gate capacitance C_0 on the other hand. For smaller capacitances C_0 we expect steeper slopes of the charge transfer. Below a minimal capacitance, $C_0 < C_{\mathrm{Min}}$, an extremal curve is reached which is symmetric around integer ν. This is the experimental situation in floating 2DES, where the NEC is only limited by the QHE breakdown.

An azimuthal current j_ϕ generates a magnetization M

$$M = \pi \int_0^R j_\phi(r) r^2 dr. \tag{1}$$

This model explains why the shape of the NECs in gated 2DESs is so different from floating 2DESs (Fig. 9). In sample B there are no input leads so the capacitance $C_0 \ll C_{\mathrm{Min}}$ and the NEC is limited only by the breakdown of the QHE.[19] In the gated sample A [Fig. 2(a)] with $C_0 > C_{\mathrm{Min}}$ the NEC is limited by the charge transfer rate. This is the reason why the NEC increases linearly with B in the regime where $\sigma_{xx}=0$ and the maximum is shifted behind the integer filling factor position with respect to the sweep direction.

If the conductivity $\sigma_{xx} > 0$ a finite relaxation current $j^{\mathrm{relax}} = \sigma_{xx} \cdot E_r$ (Fig. 8) reduces the charge redistribution. This is the case in the field regions where the NEC j^{NEC} builds up (before the slope becomes constant) and decreases (behind the region of constant slope). Investigating the gated sample A we find that the minor loops in Fig. 5 have the same slope as the extremal hysteresis at integer ν. Our model explains this fact: if one stops sweeping in the middle of the hysteresis curve, the amount of redistributed charge remains constant. Changing the sweep direction changes the direction of charge transfer so the radial electric field E_r decreases and then changes sign. We find that the NEC maxima in the extremal hysteresis and in the minor loops have the same position in the magnetic field B. This is an indication that the decrease in the NECs away from integer ν is caused by the increasing conductivity σ_{xx} as discussed above. If the conductivity is large enough the charge buildup, and with it the electric field E_r, relaxes. In contrast, in floating 2DES where the QHE breakdown limits the NEC signal the minor loops reach the extremal hysteresis curve upon change in the sweep direction. Exemplary experimental curves highlighting this effect are shown in Fig. 6 for a sample C without contacts and gate electrode.

In the model developed here the slope of the NECs depends on both the filling factor and the gate capacitance C_0. C_0 is constant in our experiment. At high magnetic fields $B_\perp > 3.8$ T at $\nu=2$ the slope of the NECs is found to be constant for different carrier densities n_S in Fig. 4(a). We attribute this to a very low conductivity σ_{xx} that does not support a significant relaxation current. At magnetic fields, $B_\perp < 3.8$ T, the conductivity becomes $\sigma_{xx} \gg 0$ so that the NEC is reduced due to the relaxation of E_r. No NECs are observed below $B_\perp < 2.7$ T.

Up to now we have discussed the origin and the shape of NECs in a sweeping magnetic field. While it is quite intuitive that a variation in B induces NECs it is at a first glance rather surprising that also a variation in n_S induces NECs as shown in Fig. 4(b). In the following we show that the model developed above gives a consistent description of this experimental finding. In Fig. 8(b) at integer ν the bulk of the sample is incompressible. As a consequence the carrier density n_S can only be changed in the compressible strips at the sample edge. This generates a self-consistent shift of the compressible and incompressible strips leading to a radial electric field E_r which drives the NEC j^{NEC}. If we assume that the radial electric field E_r is proportional to the swept gate voltage difference ΔV_{gate} in which σ_{xx} is small enough, we find that the NEC j^{NEC} depends linearly on the carrier density difference Δn_S in this regime

$$j^{\mathrm{NEC}} = \sigma_{xy} E_r \propto \Delta V_{\mathrm{gate}} \propto \Delta n_S. \tag{2}$$

The resulting profile of the electrostatic energy V is the same as in the magnetic-field-dependent measurement [Fig. 8(c)]. Comparing NECs induced by $\partial n_S / \partial t$ at different magnetic fields $B_\perp > 3.8$ T one finds indeed a constant slope [Fig. 4(b)] as predicted by this model. At small magnetic fields $B_\perp < 3.8$ T the NECs are reduced due to a finite σ_{xx} and the accompanying relaxation of E_r. Below $B_\perp < 2.7$ T the NECs have vanished.

Comparing the asymmetric shape of the NECs induced by sweeping B in Fig. 4(a) and by sweeping n_S in Fig. 4(b) one finds a striking similarity: as shown in Fig. 10 indeed both NECs have an identical shape when plotted against the filling factor ν. This underscores the similarity of the mechanism of generation of the NECs: the NECs are always driven by a radial electric field. Only the origin of the radial field differs for sweeping B or sweeping n_S. In the former it originates from a radial charge current driven by the $\partial B / \partial t$-induced azimuthal electric field while in the latter it is due to the charge injected from the contacts.

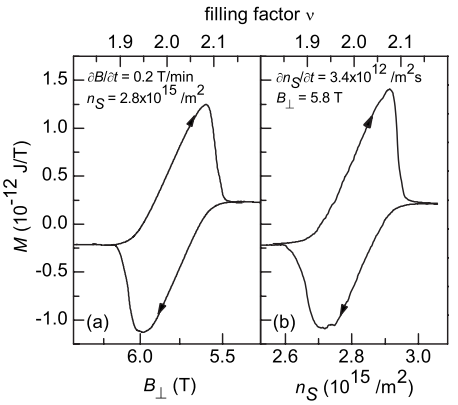

FIG. 10. Magnetization M for (a) sweeping the magnetic field $\partial B/\partial t$ and (b) sweeping the carrier density $\partial n_S/\partial t$ at $T=300$ mK. Arrows indicate the sweep direction. Both NECs have the same shape if plotted against the total filling factor ν. Slight differences in the noise level will be addressed in Sec. V C.

V. APPLICATION OF THE MODEL

A. Temperature dependence of NECs

In this section we present temperature-dependent measurements of the NEC amplitude ΔIA in sample A defined as

$$\Delta IA = \max\left[M\left(\frac{d\nu}{dt}<0\right) - M\left(\frac{d\nu}{dt}>0\right)\right], \tag{3}$$

i.e., as the maximum of the difference of down and up sweep magnetization M. We have chosen the parameter ΔIA for the amplitude of the NECs to separate it clearly from ΔM which is reserved in the literature for the amplitude of the dHvA oscillations. ΔIA was evaluated as a function of temperature T at a fixed carrier density n_S and a fixed sweep rate of the magnetic field $\partial B/\partial t$ [Fig. 4(a)]. The temperature dependence of ΔIA is shown in Fig. 7(b). We determined the relation between conductivity $\sigma_{xx}(T)$ and the NEC amplitude $\Delta IA(T)$ via simultaneous measurement of the longitudinal resistance.

This was done in the following way: Fig. 7(c) shows the longitudinal resistance minimum at filling factor $\nu=2$. The data were fitted with a reciprocal Gaussian

$$R_{xx}(B) = R_{\text{parasit}} + R^0_{xx}\left\{\exp\left[-\left(\frac{B-B_0}{2\Gamma}\right)^2\right]\right\}^{-1} \tag{4}$$

to evaluate the minimum R^0_{xx} and the width $\Delta B_\perp$ of the R_{xx} plateau with $R_{xx}<R_{xx,\text{crit}}$. Here, $R_{xx,\text{crit}}$ is defined as the critical resistance where the NEC signal reduces to zero, i.e., where the hysteretic M_{NEC} curves for different sweep directions meet [Fig. 11(a)]. The offset R_{parasit} is caused by a parasitic parallel conductance due to the continuous laser illumination from the laser interferometer during the magnetization measurement. Nevertheless the longitudinal resistance exhibits a pronounced plateau-shaped minimum. We note that after cooling down without laser illumination the plateau value reaches zero. From this we conclude that longitudinal-transverse mixing in the van der Pauw measurements does not contribute significantly to the resistance offset R_{parasit}.

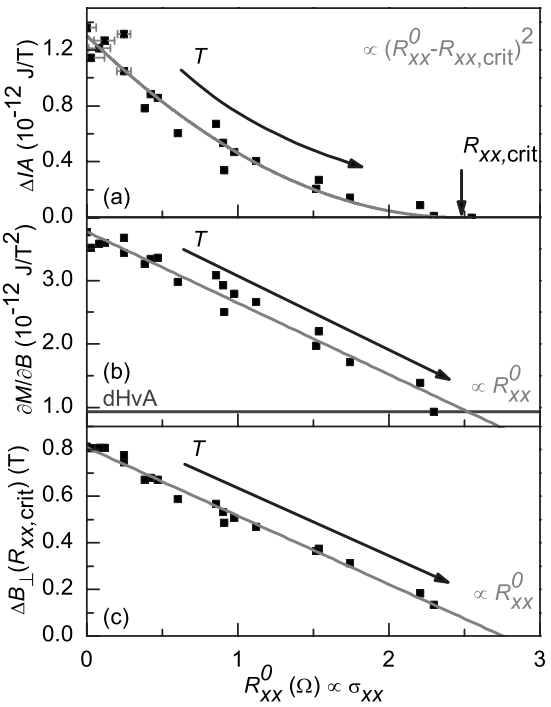

FIG. 11. (a) NEC amplitude ΔIA from Fig. 7(b) plotted as a function of the temperature-dependent longitudinal resistance R^0_{xx} (at integer ν). Above $R^0_{xx}>R_{xx,\text{crit}}$ no NECs are observed. A quadratic dependence on $R^0_{xx}-R_{xx,\text{crit}}$ is found. This is explained by the data in (b) and (c): the slope $\partial M/\partial B$ (b) of the NECs depends linearly on R^0_{xx}, due to the linear dependence on the relaxation current. The minimal slope of the signal is not zero, but corresponds to the slope of the dHvA effect. (c) The width $\Delta B_\perp$ of the region where $R_{xx}<R_{xx,\text{crit}}$, i.e., the width of the longitudinal resistance minimum in Fig. 7(c), is also linearly dependent on R^0_{xx}. These two effects combined yield the quadratic dependence on R^0_{xx}.

We now apply the model developed above to the observed T dependence of ΔIA: the reduction in amplitude with increasing T is due to the increase in σ_{xx} with increasing T. This leads to a relaxation current j^{relax} which reduces the charge redistribution and thereby the radial electric field. The relaxation current is directly proportional to the longitudinal conductivity σ_{xx}. In contrast, in Refs. 17 and 35, the T dependence of the NEC amplitude of a floating 2DES was believed to be dominated by the modification of the breakdown of the QHE with temperature.

In the QH state at integer ν the longitudinal conductivity σ_{xx} is proportional to the longitudinal resistivity ρ_{xx} (Ref. 36) which in our case is proportional to the van der Pauw resistance R_{xx} measured in the experiment. Figure 11(a) highlights the experimentally observed dependence of the NEC amplitude ΔIA on the conductivity σ_{xx}. The conductivity σ_{xx} increases with rising temperature T which results in decreasing NEC amplitudes ΔIA. No NECs are observed above $R_{xx,\text{crit}}$. We observe a quadratic dependence of ΔIA on σ_{xx} which we explain with two contributions: on the one hand the slope of the NECs $\partial M/\partial B$ decreases linearly with σ_{xx} in Fig. 11(b). Here, the minimal slope is not zero but the slope of the underlying de Haas–van Alphen effect. On the other hand, we find a linear dependence of the width $\Delta B_\perp$ of the

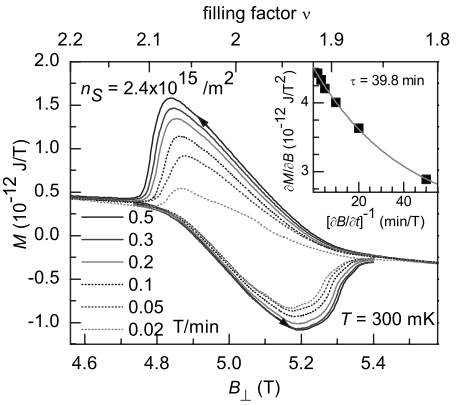

FIG. 12. Magnetization M of NECs for different sweep rates $\partial B/\partial t$ at $T=300$ mK. The slope $\partial M/\partial B$ of the increasing NEC signal at integer ν plotted against the reciprocal sweep rate shows an exponential decrease (inset). The solid line is a fit to the equivalent circuit model described in the text and corresponds to a decay time of 39.8 min.

longitudinal resistance minimum with $R_{xx}<R_{xx,\mathrm{crit}}$ corresponding to the width of the NEC [Fig. 11(c)]. These two linear relations add up to the quadratic relationship between conductivity σ_{xx} and ΔIA.

If we assume the Arrhenius formula for the T dependence of $R_{xx,0}=R_0\exp[-\Delta E/2k_BT]$ we have

$$\Delta IA = A_1\left[R_0\exp\left(-\frac{\Delta E}{2k_BT}\right)-R_{xx,\mathrm{crit}}\right]^2. \tag{5}$$

Here, the prefactor $A_1=2.13\times10^{-13}$ J/T Ω^2 and the critical resistance $R_{xx,\mathrm{crit}}=2.48$ Ω are obtained from the fit in Fig. 11(a). As results of the Arrhenius plot we find $R_0=7.62$ Ω and $\Delta E/2k_B=4.56$ K. The curve resulting from these four parameters is shown as a gray line in Fig. 7(b) and reproduces the data very well. We emphasize here that this is not a fit to the data in Fig. 7(b). The parameters have been determined directly from the evaluations shown in Fig. 11.

These data obtained by simultaneous magnetization and magnetotransport measurements reveal a direct relation between the NEC amplitude and the longitudinal conductivity σ_{xx}. The observed dependence of the NEC amplitude on the experimental parameter σ_{xx} and on the temperature is consistently explained in the framework of our model.

B. NECs at different sweep rates

In this section we discuss the sweep-rate dependence of the NECs (Fig. 12). The NEC amplitude shows only a very weak dependence on the sweep rate $\partial B/\partial t$ in the gated sample. The slope $\partial M/\partial B$ of the increasing NEC at integer ν decreases exponentially with the reciprocal sweep rate $[\partial B/\partial t]^{-1}$ (Fig. 12, inset). The observed behavior is in contrast to floating 2DESs.[12]

To explain these findings we transform our model into an equivalent circuit diagram. A capacitor C_0 [charge redistribution, see Fig. 8(a)] with a parallel resistance $R\propto\sigma_{xx}^{-1}$ (relaxation via j^{relax}) is charged by a constant radial current j_r. The radial electric field E_r driving the NECs is proportional to the voltage drop V_C over the capacitor. The equivalent circuit diagram yields for the saturation curve of V_C

$$M\propto j_\phi\propto E_r\propto V_C(t)=R\cdot j_r\left[1-\exp\left(-\frac{t}{RC_0}\right)\right]. \tag{6}$$

The current j_r charging the capacitor C_0 is proportional to the constant sweep rate $\partial B/\partial t$

$$M(B)\propto\frac{\partial B}{\partial t}\left\{1-\exp\left[-\frac{B\cdot(\partial B/\partial t)^{-1}}{RC_0}\right]\right\}. \tag{7}$$

The derivative with respect to B leads to

$$\frac{\partial M}{\partial B}\propto\exp\left[-\frac{\Delta t(\Delta B=\mathrm{const.})}{RC_0}\right]. \tag{8}$$

Here, $\Delta t(\Delta B=\mathrm{const.})$ denotes the time needed for sweeping a fixed magnetic-field increment, which is proportional to the reciprocal sweep rate $[\partial B/\partial t]^{-1}$. In other words the more time is needed to sweep over the field interval ΔB the smaller is the slope of the NECs because the charge redistribution has more time to relax via j^{relax}.

Assuming an ideal 2DES with $\sigma_{xx}\equiv0$ and $R=\infty$ meaning $j^{\mathrm{relax}}=0$ our equivalent circuit model predicts the same slope $\partial M/\partial B$ for all sweep rates $\partial B/\partial t$. In this case, the amplitude of the NECs ΔIA would not depend on the sweep rate $\partial B/\partial t$. In our case with $\sigma_{xx}>0$ the model predicts an exponential decrease in the slope $\partial M/\partial B$ with increasing reciprocal sweep rate $[\partial B/\partial t]^{-1}$. This is indeed observed in the experiment: in the inset of Fig. 12 the experimental values of $\partial M/\partial B$ at integer ν are plotted as filled symbols. The solid gray line is a fit according to Eq. (8) and is in agreement with the experimental data. In our gated 2DES, the sweep-rate dependence of the NECs is thus due to the competition of the induced radial charging current and the finite relaxation current due to $\sigma_{xx}>0$.[37]

C. Noise in magnetometry on NECs

A few additional points are worth noting when discussing the role of the contacts in NEC generation: in Fig. 10 the NECs for sweeping the field and sweeping the carrier density were compared. Despite the striking similarity two minor but reproducible differences are present. (i) The NEC minimum in the n_S-dependent down sweep (discharging the 2DES) is somewhat truncated in comparison to the minimum in the B-dependent down sweep. The maximum (charging the 2DES) is less affected. One may speculate that this difference might be due to a local depletion of the 2DES edge when draining charge from the 2DES. It seems that it is easier to add charge to the system close to an integer ν, than to deplete it beyond a certain point. A closer look at the data in Fig. 10 reveals further intriguing details of the charging and discharging effects: for this, the noise δM of the NEC signal when B is swept and when n_S is swept is displayed in Fig. 13. Here, the incline of the NEC signal has been subtracted from the data. As one can see, the noise is strongly enhanced around integer ν when varying n_S but not when varying B.[38] To rule out noise in the gate voltage as a source we show for comparison the noise level away from integer ν

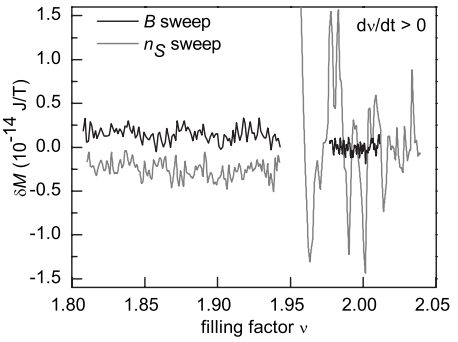

FIG. 13. Comparison of the noise δM of the NEC signal when B is swept (black) and when n_S is swept (gray). To extract δM we subtracted a linear fit from the magnetization signal around $\nu=2$ in Fig. 10 (right). The noise δM is strongly enhanced when n_S is swept. To exclude possibly different noise pickup due to the different measurement setup when a voltage source is connected to the gate and 2DES we analyze δM also in between integer ν, where no NECs are present (left). Here, no difference between a B sweep and a n_S sweep is resolved in δM.

on the left of Fig. 13 for both cases. Here, no difference is resolved between varying n_S and varying B. The increased noise level thus seems to be connected to the charging and discharging of the 2DES via the contacts: away from integer ν a smooth charging of the 2DES is possible. Around integer ν, where NECs are present in the system, charging or discharging seems to be accompanied by additional fluctuations. We have no microscopic picture for this effect up to now. However, one difference between the n_S sweep and the B sweep is that in the latter the NEC is generated contactless via the induced E_ϕ field. Here, the relevant conductivity is quantized. In the former the field driving the NECs is generated via the contacts. Charges are added and removed via the contact resistance that is not quantized and scattering across the edge strips must be involved.[32] A microscopic picture of the charge transport from the contact across the reconstructed edge region would be necessary to understand these features in detail. This is beyond the scope of the present paper.

VI. CONCLUSION

In conclusion we have investigated the magnetic signals arising from NECs induced by both $\partial n_S/\partial t$ and $\partial B/\partial t$ in a gated 2DES. We have developed a capacitive charging model that sheds light on the mechanisms of the NEC generation in both cases. The model consistently explains the experimental observations including the shape, temperature dependence and the dependence on sweep rate. In strong contrast to NECs in floating 2DES we have shown that the NECs in the gated system are not limited by the breakdown of the quantum Hall effect, but by the gradual buildup of the radial Hall field limited by the gate capacitance. *In situ* resistance measurements enabled us to directly relate the NEC signals to the resistance of the 2DES. In particular, the constant slope of the NEC signal for a given ν directly reflects the conductance quantization. The experiments show that the NECs are decoupled from the contacts and do not interact with the transport currents of the quantum Hall effect.

ACKNOWLEDGMENTS

The authors thank A. Schwarz for continuous support and T. Matsuyama for fruitful discussions. We acknowledge financial support by the Deutsche Forschungsgemeinschaft via SFB 508, the Excellence Cluster Nanosystems Initiative Munich and the Schwerpunktprogramm 1285 via Grant No. GR1640/3.

*Present address: Institut für Festkörperphysik, Technische Universität Berlin, Hardenbergstraße 36, D-10623 Berlin, Germany.
†mwilde@ph.tum.de

[1] S. A. J. Wiegers, M. Specht, L. P. Levy, M. Y. Simmons, D. A. Ritchie, A. Cavanna, B. Etienne, G. Martinez, and P. Wyder, Phys. Rev. Lett. **79**, 3238 (1997).
[2] M. P. Schwarz, M. A. Wilde, S. Groth, D. Grundler, C. Heyn, and D. Heitmann, Phys. Rev. B **65**, 245315 (2002).
[3] M. Zhu, A. Usher, A. J. Matthews, A. Potts, M. Elliott, W. G. Herrenden-Harker, D. A. Ritchie, and M. Y. Simmons, Phys. Rev. B **67**, 155329 (2003).
[4] M. A. Wilde, M. Rhode, C. Heyn, D. Heitmann, D. Grundler, U. Zeitler, F. Schäffler, and R. J. Haug, Phys. Rev. B **72**, 165429 (2005).
[5] I. Meinel, T. Hengstmann, D. Grundler, D. Heitmann, W. Wegscheider, and M. Bichler, Phys. Rev. Lett. **82**, 819 (1999).
[6] S. A. J. Wiegers, M. Specht, E. D. Bibow, L. P. Lévy, S. Melinte, E. Grivei, V. Bayot, M. Y. Simmons, D. A. Ritchie, M. Shayegan, A. Cavanna, C. Etienne, G. Martinez, and P. Wyder, Physica B **256-258**, 16 (1998).
[7] M. A. Wilde, M. P. Schwarz, C. Heyn, D. Heitmann, D. Grundler, D. Reuter, and A. D. Wieck, Phys. Rev. B **73**, 125325 (2006).
[8] M. A. Wilde, D. Reuter, C. Heyn, A. D. Wieck, and D. Grundler, Phys. Rev. B **79**, 125330 (2009).
[9] D. Shoenberg, *Magnetic Oscillations in Metals* (Cambridge University Press, Cambridge, England, 1984).
[10] D. Shoenberg, J. Low Temp. Phys. **56**, 417 (1984).
[11] M. A. Wilde, J. I. Springborn, O. Roesler, N. Ruhe, M. P. Schwarz, D. Heitmann, and D. Grundler, Phys. Status Solidi B **245**, 344 (2008).
[12] C. L. Jones, A. Usher, M. Elliott, W. G. Herrenden-Harker, A. Potts, R. Shepherd, T. S. Cheng, and C. T. Foxon, Solid State Commun. **97**, 763 (1996).
[13] C. L. Jones and A. Usher, Solid State Commun. **95**, 409 (1995).
[14] A. J. Matthews, J. P. Watts, M. Zhu, A. Usher, M. Elliott, W. G. Herrenden-Harker, P. R. Morris, M. Y. Simmons, and D. A. Ritchie, Physica E (Amsterdam) **6**, 140 (2000).
[15] M. P. Schwarz, D. Grundler, C. Heyn, D. Heitmann, D. Reuter, and A. D. Wieck, Phys. Rev. B **68**, 245315 (2003).
[16] A. J. Matthews, K. V. Kavokin, A. Usher, M. E. Portnoi, M. Zhu, J. D. Gething, M. Elliott, W. G. Herrenden-Harker, K. Phillips,

D. A. Ritchie, M. Y. Simmons, C. B. Sorensen, O. P. Hansen, O. A. Mironov, M. Myronov, D. R. Leadley, and M. Henini, Physica E (Amsterdam) **22**, 201 (2004).

[17] A. J. Matthews, K. V. Kavokin, A. Usher, M. E. Portnoi, M. Zhu, J. D. Gething, M. Elliott, W. G. Herrenden-Harker, K. Phillips, D. A. Ritchie, M. Y. Simmons, C. B. Sorensen, O. P. Hansen, O. A. Mironov, M. Myronov, D. R. Leadley, and M. Henini, Phys. Rev. B **70**, 075317 (2004).

[18] A. J. Matthews, A. Usher, and C. D. H. Williams, Rev. Sci. Instrum. **75**, 2672 (2004).

[19] A. Usher and M. Elliott, J. Phys.: Condens. Matter **21**, 103202 (2009).

[20] It should be noted here that asymmetric NECs have also been reported in a floating 2DES with a very high mobility by Matthews *et al.* (Ref. 39) and have also been observed by the present authors. However, the asymmetry observed in these floating samples shows a behavior that is completely different from the behavior reported in the present paper: a steep increase in the eddy current before the integer ν, where the maximum is reached before the integer filling, followed by a long decrease with small slope. A model for the asymmetric shape in these floating samples was developed in Ref. 39. In this paper we focus on NECs in a gated 2DES. Here, the asymmetry is the other way round: a long increase with constant slope that extends behind the position of integer ν. The decrease only starts behind the position of integer filling.

[21] D. R. Faulhaber and H. W. Jiang, Phys. Rev. B **72**, 233308 (2005). We note that one must introduce a minus sign to the magnetization M in Figs. 1 and 3 of this reference to reproduce the correct paramagnetic-to-diamagnetic jumps of the dHvA effect. This change in sign is relevant and must be considered for the conclusions drawn in this former work.

[22] V. T. Dolgopolov, A. A. Shashkin, N. B. Zhitenev, S. I. Dorozhkin, and K. von Klitzing, Phys. Rev. B **46**, 12560 (1992).

[23] J. Huels, J. Weis, J. Smet, K. v. Klitzing, and Z. R. Wasilewski, Phys. Rev. B **69**, 085319 (2004).

[24] T. Klaffs, V. A. Krupenin, J. Weis, and F. J. Ahlers, Physica E (Amsterdam) **22**, 737 (2004).

[25] N. Ruhe, J. I. Springborn, C. Heyn, M. A. Wilde, and D. Grundler, Phys. Rev. B **74**, 235326 (2006).

[26] J. I. Springborn, N. Ruhe, C. Heyn, M. A. Wilde, D. Heitmann, and D. Grundler, Physica E (Amsterdam) **34**, 172 (2006).

[27] M. P. Schwarz, D. Grundler, I. Meinel, C. Heyn, and D. Heitmann, Appl. Phys. Lett. **76**, 3564 (2000).

[28] V. A. Guzenko, T. Schäpers, and H. Hardtdegen, Phys. Rev. B **76**, 165301 (2007).

[29] D. B. Chklovskii, B. I. Shklovskii, and L. I. Glazman, Phys. Rev. B **46**, 4026 (1992).

[30] M. R. Geller and G. Vignale, Phys. Rev. B **50**, 11714 (1994).

[31] E. Ahlswede, P. Weitz, J. Weis, K. von Klitzing, and K. Eberl, Physica B **298**, 562 (2001).

[32] E. Ahlswede, J. Weis, K. von Klitzing, and K. Eberl, Physica E (Amsterdam) **12**, 165 (2002).

[33] R. R. Gerhardts, Phys. Status Solidi B **245**, 378 (2008).

[34] M. R. Geller and G. Vignale, Physica B **212**, 283 (1995).

[35] K. Kavokin, M. Portnoi, A. Matthews, A. Usher, J. Gething, D. Ritchie, and M. Simmons, Solid State Commun. **134**, 257 (2005).

[36] T. Chakraborty and P. Pietiläinen, *The Fractional Quantum Hall Effect: A Survey of the Incompressible Quantum Fluid Including the Integer Quantum Hall Effect* (Springer, Berlin, 1995).

[37] We do not address the absolute signal strength of NECs by our modeling. To do so, one might also take into account effects introduced by R_{parasit}. However, the good qualitative agreements between experimental data and modeling suggests that such effects, if present, are of minor importance.

[38] This is different from the observations in Ref. 40, where the authors observed a "noisy" behavior of NECs in a contact-free geometry which they attributed to an avalanche-type breakdown of the quantum Hall effect.

[39] A. J. Matthews, K. V. Kavokin, A. Usher, M. E. Portnoi, J. D. Gething, M. Zhu, and D. A. Ritchie, Int. J. Mod. Phys. B **18**, 3593 (2004).

[40] M. Elliott, Y. Lu, K. L. Phillips, W. G. Herrenden-Harker, A. Usher, A. J. Matthews, J. D. Gething, M. Zhu, M. Henini, and D. A. Ritchie, Europhys. Lett. **75**, 287 (2006).